General Disclaimer

One or more of the Following Statements may affect this Document

- This document has been reproduced from the best copy furnished by the organizational source. It is being released in the interest of making available as much information as possible.

- This document may contain data, which exceeds the sheet parameters. It was furnished in this condition by the organizational source and is the best copy available.

- This document may contain tone-on-tone or color graphs, charts and/or pictures, which have been reproduced in black and white.

- This document is paginated as submitted by the original source.

- Portions of this document are not fully legible due to the historical nature of some of the material. However, it is the best reproduction available from the original submission.

GAMMA RAY ASTRONOMY BALLOON RESULTS

C. E. Fichtel

D. A. Kniffen

H. B. Ögelman

February 1969

GAMMA RAY ASTRONOMY BALLOON RESULTS

C. E. Fichtel, D. A. Kniffen, and H. B. Ögelman
NASA/Goddard Space Flight Center, Greenbelt, Md.

ABSTRACT

The results obtained from recent high altitude balloon flights of the Goddard gamma ray digitized spark chamber telescope are reported and combined with earlier work. The data on the galactic center region is reanalyzed in terms of a possible line source in the galactic plane. The analysis leads to a value of $(2.3 \pm 1.2) \times 10^{-4} \gamma /(cm^2 \, sec \, rad)$ above 100 MeV for a galactic latitude interval of $-3°$ to $+3°$ in the galactic center region; this result in itself does not justify the claim of a detected flux, but is consistent with the line intensity of $(4.1 \pm 0.7) \times 10^{-4} \gamma /(cm^2 sec \, rad)$ quoted from recent OSO-III results (Clark et al., 1969). The flux and energy spectrum of the atmospheric background were measured as a function of angle with respect to the vertical. The measured downward flux is in reasonable agreement with measurements of other experimenters at several energies; however, the upward flux for energies above 100 MeV is a factor of about three lower than that measured in the OSO-III experiment mentioned above. This difference seems larger than would be expected, but small compared to the difference between the galactic gamma-ray flux observed by OSO-III and the predicted one. The upper limits to possible point sources of gamma rays are summarized and shown generally to fall below the fluxes expected from a straight extrapolation of the x-ray spectra. No positive evidence for a point source has been found.

I. INTRODUCTION

Current cosmic ray data and radio astronomical measurements indicate that relativistic particles constitute a significant fraction of the total energy in the environment of various celestial objects and in some regions of our galaxy and the universe. Gamma rays are intimately related to relativistic electrons, and high energy nuclear processes. Electrons may radiate γ-rays by the synchrotron process as they are deflected by magnetic fields, by bremsstrahlung as they pass through matter, and by the inverse Compton effect when they interact with photons. In high energy interactions of baryons, gamma rays may be produced as the decay products of hyperons and mesons, such as the pions formed in the interaction of cosmic rays with interstellar matter and matter-antimatter annihilation.

The study of high energy photons is necessarily a new field of astrophysics since the short path length of these quanta in air make it necessary to place the observing instruments near the top of the atmosphere. Further, the fluxes are now known to be small, and at present there has been no certain measurement of high energy γ-rays (E > 30 MeV) from any point source. However, Clark, Garmire, and Kraushaar (1968) have obtained positive evidence for a celestial γ-ray flux which is anisotropic with a higher intensity in the direction of the galactic plane and a maximum in the galactic center region. The flux measured in the galactic plane is more than an order of magnitude greater than that expected from the interaction of cosmic rays with interstellar matter, magnetic fields, and photons.

1

In this paper we shall summarize gamma ray balloon flight results related to several topics including: (a) present balloon flight results on the gamma radiation from the atmosphere, coming upwards, from just below the horizon, and downward at balloon altitudes, (b) give the upper limit obtained on the flux from M-87, and summarize the upper limits from point sources obtained thus far, and (c) review the galactic center data reported previously (Fichtel, Cline, Ehrmann, Kniffen, and Ross, 1968) in light of the new results of Clark et al. (1968). The atmospheric gamma radiation is of interest both from the standpoint of providing a means of determining its specific origin and for the in-flight cali- bration of gamma-ray satellite experiments. As a background for this discussion the detector system will be briefly described, and an account of the method of data analysis will be given. The latter is particularly important in terms of understanding the upper limits obtained for the possible sources of gamma radiation.

II. EXPERIMENTAL APPROACH

For high energy gamma rays, the dominant interaction process is the con- version to a negatron positron pair. The average angle between the pair tends to decrease with increasing energy, because it is primarily determined by elec- tron scattering. Information on the direction and energy of the gamma ray must be derived from this pair since the penetration power of gamma-rays and their low flux relative to other possible masquerading events make shielding difficult and generally undesirable.

A good gamma ray telescope must discriminate against charged particles with a high efficiency, give enough information to select gamma rays from other

2

neutral events, permit accurate determination of the gamma ray's arrival direction, provide a means of measuring the gamma ray's energy, and, at the same time, have a reasonably large detection probability. The detector system used in these experiments is shown in Figure 1. The large plastic scintillator anticoincidence dome together with the directional Cerenkov counter is employed to restrict the analysis to downward moving particles and discriminate against charged particles. The spark chamber satisfies the need for a large volume high information content detector to permit selection of the gamma rays and measure the properties of the negatron-positron pair. The central plastic scintillator together with the Cerenkov counter in coincidence and the plastic dome in anticoincidence provides the information to determine whether or not the spark chamber should be triggered. The bell shaped anticoincidence dome is a solid piece of plastic scintillator, 5/8" thick.

The spark chamber itself, the associated electronics, and the advantages of a digitized spark chamber are discussed in detail in another article (Ehrmann, Fichtel, Kniffen, and Ross, 1967); so only the principal features will be given here. As shown in Figure 1, the spark chamber consists of two units separated by the central scintillator. Each unit consists of a series of fifteen plates and sixteen 6" by 6" wire-grid modules. Each of these modules is a frame-wire assembly consisting of two orthogonal sets of 128 wires each. One orthogonal wire grid serves as the high voltage plane of the modular unit, the other as the ground plane. The bottom module in each chamber differs from the others in that the wires run at an angle of 45° with respect to the others, in order to allow the removal of the ambiguity related to which x reading is associated with which

3

y reading when two tracks are present. The spark chamber gas is 88-1/2% neon, 10% helium, 1% argon, and 1/2% alcohol and is at a pressure of 1-1/2 atmospheres.

Since the spark is formed between the two wire grids in each x-y module, there is no spark robbing, as there is when the pair-producing plates serve as the electrodes. In the double wire grid system, an x and y reading for each spark is obtained from each modular unit with high efficiency even for multiple track events. Each of the grid wires in the spark chamber threads a magnetic core, which receives and contains its datum of information when the high voltage is pulsed to the chamber plates. The cores are normally in the quiescent, or "reset," state between operations. Spark current in a wire "sets" a core, and the "readout" act of determining which cores have been set by the events resets the cores. The mean uncertainty in the position of the particle trajectory at any level is approximately 0.4 mm.

Each of the 30 pair producing plates consists of .02 radiation length of gold plated unto a .002 radiation length base of aluminum, thus providing a high Z plate which is thin enough so that the character of the event is not destroyed by absorption and Coulomb scattering of the electrons, and the direction of the incident gamma ray can be measured well. At the same time, the large number of plates retains a reasonably large detection efficiency. Finally, information on the energy of the negatron and positron can be obtained from the multiple coulomb scattering in the plates.

For the flights looking at point sources, the gamma ray telescope is placed in a gondola at a fixed angle with respect to the vertical and the gondola itself is

4

oriented with respect to the geomagnetic field to an accuracy of about ±1/2°.
The orientation is achieved with the aid of two pairs of gas jets supported on
booms at each end of the gondola. A flux gate magnetometer is mounted into the
gondola in a manner so that a zero reading will occur when the gamma ray tele-
scope axis is in the north-south plane. The signal from the magnetometer is
used both for orientation data, together with two other magnetometers, and for
jet activation if a pointing error greater than about a half degree is detected.

For the flight looking at the earth albedo, the detector was first set in the
gondola pointing at an angle of 112° with respect to the vertical. After one hour
exposure at ceiling with this position, the detector was lowered to an angle of
172° with respect to the vertical. With the given opening angle of the detector,
sets of angles with respect to the zenith of approximately 95° to 130° and 155° to
180° could be studied.

III. DATA REDUCTION

Energy, Arrival Direction, and Flux Calculations

In order to describe the energy measurement, the accuracy of the arrival
direction, and also the flux calculation, particularly at low energy, it is neces-
sary to review first the combined effects of multiple coulomb scattering in the
spark chamber plates and energy loss by the electrons. The theory of multiple
coulomb scattering has been analyzed in detail by Williams (1939), Molière (1947,
1948, 1955), and others (Goudsmit and Saunderson, 1940; Snyder and Scott, 1949;
Scott, 1952; Bethe, 1953) and applied successfully for many years to the energy
determination of charged particles in nuclear emulsions and cloud chambers.

5

More recently the method has been applied to multiplate spark chambers by Pinkau (1966, 1967) and extended to overlapping cells by Kniffen (1967).

Attempts to take energy loss into account have been made by Kniffen (1967) using the average energy and by Pinkau (1968) using an average rate of energy loss. For the high nuclear charge material comprising the plates of this experiment radiation losses (bremsstrahlung) predominate over ionization losses above 10 MeV and ionization losses predominate below 10 MeV. Including the effect of scattering, the energy loss tends to be relatively independent of energy below about 25 MeV, whereas above that energy it is proportional to the electron's energy. Whereas the ionization energy loss is a smooth function, the radiation loss is not and can vary significantly in any one case. For this reason and because of the statistical uncertainty of the energy measurement, either the approach of Kniffen (1967) or Pinkau (1968) is adequate.

Figure 2 defines the geometry used in the coulomb scattering analysis. The pv value of the electron, for the case when energy loss is neglected, is given by the expression (Pinkau, 1967):

$$p v = 16.5 \, Q_n / < |\beta_{sn}| > , \tag{1a}$$

where

$$Q_n^2 = \frac{n}{2} d \left(\Delta^2 + \frac{d^2}{3} \right) + \frac{2}{3} (n + 1) n (n - 1) \Delta^2 d, \tag{1b}$$

and

$$< |\beta_{sn}| > = < | x_{ni} - 2x_{n(i-1)} + x_{n(i-2)} | > , \tag{1c}$$

6

where d = 0.0004 cm and Λ = 0.75 cm for this spark chamber, n is the number of plates in a cell, p is the particle momentum, and v is its velocity. The β_n in this expression is the result only of coulomb deflections. In practice there is also a noise signal, called N, which is essentially independent of energy and results from fluctuations of the spark from the track location and the minimum accuracy for determining x_n. For this experiment, N was 1.0 mm. The measured signal β_{mn} is given by the following relationship:

$$< |\beta_{mn}| >^2 \doteq < |\beta_{sn}| >^2 + < |N| >^2 . \tag{2}$$

$< |N| >$ may be determined by calibration or by eliminating it using the overlapping cell method (Fowler, 1950); the former method was used here since it (a) permits using only n = 1 where that is appropriate and (b) gives a more accurate measure of $< |N| >$ on the average.

In practice, calibration data on electrons of known energy were used to obtain experimental curves of $< |\beta_{mn}| >$ vs. electron energy. This was done for each deck in the top half of the chamber, where, in each case, all readings arising from data taken above that deck were eliminated in determining $< |\beta_{mn}| >$ and the result plotted against the most probable energy of the electron at that deck. Thus we obtain calibration curves for the determination of the energy of any electron formed in the conversion of a gamma-ray at any level in the top half of the chamber. In this manner an energy estimate of each electron is obtained (Note: since v $\approx$ c, pv $\approx$ E), and the energy of the gamma ray is obtained by adding them with the uncertainty in the gamma ray energy being the square root of the sum of the squares of the uncertainties in the individual energies. The uncertainty

in the gamma ray energy typically varies from 30% at the lowest energies to a factor of 2 at about 150 MeV.

The arrival direction of the gamma ray is determined from the knowledge of each electron's energy and direction in the following manner. First, on the basis of the energy estimate of the electron, a determination is made of the number of plates, m, through which the electron must pass before $<|\beta_{sn}|>$ is equal to $<|N|>$. Then, a least squares fit is made to each electron through the m plates, beginning at the apex of the pair. This approach provides the maximum information on track location (Kniffen, 1967), unless a point weighting method is used (Pinkau, 1968). The latter improves the accuracy somewhat, but greatly increases the data reduction time. The projected angles of the gamma ray in the two orthogonal projections are then calculated as follows $\phi_{x\gamma}$ is given by the expression

$$\phi_{x\gamma} = (\omega_1 \phi_{x1} + \omega_2 \phi_{x2}) \frac{1}{(\omega_1 + \omega_2)} \tag{3}$$

where ϕ_{xj} is the projected angle of the jth electrons and ω is the statistical weight of the ϕ_{xj} determination, which is analyzed in Appendix I and given by:

$$\omega_{1,2} = \sigma_{2,1}^2 \tag{4}$$

where

$$\sigma_{2,1} = \sqrt{\frac{12}{k_{2,1}^3 - k_{2,1}} \left(\xi_d^2 W_{ni} + 2\alpha^2\right)}$$

and α is the r.m.s. error in the x measurement which is 0.5 mm and $k_{2,1}$ is the number of plates for which $<|\beta_{sn}|> = <|N|>$. $\xi_d^2 W_{ni}$ is defined in Appendix I.

The accuracy of the determination of the arrival direction can be calculated from the lateral displacement function for each electron (Pinkau 1966, 1967). The final angular errors quoted are those within which 95% of the true gamma ray arrival directions will lie.

Above about 120 MeV, the arrival direction is determined by the bisector of the pair and the uncertainty in arrival direction at very high energies (> 1000 MeV) is limited mostly by the track location accuracy. In addition, there is also an inherent small angle between the direction of the electron and the primary gamma ray due to the pair producing interaction. When both electrons are taken into account, the error introduced is about 0.3 of the above errors in each case (Stearns, 1949). Since the uncertainties add in a random way, this latter effect increases the uncertainty by only about 5%. A curve showing the uncertainty in arrival direction as a function of the primary gamma ray energy is shown in Figure 3.

Knowing the balloon gondola angles, the balloon location, and the time, the conversion from the angles in the spark chamber to celestial coordinates, or angles with respect to the vertical in the case of the albedo and atmospheric secondary studies can then be accomplished in a straight forward manner (Kniffen, 1967).

In order to determine the absolute value of the flux of gar ia rays, it is necessary to determine the efficiency for detection as a function of energy and the angle of the detector with respect to the direction of interest. At high energies, the efficiency is simply a product of the pair production probability and

9

the fraction of the sensitive area exposed to the source. At the low energies the efficiency is affected both by the energy loss of the electrons in the chamber and electron scattering which causes some electrons to be scattered into and out of the cone of acceptance. This effect is considered in detail by Kniffen (1967) with the net result being to increase slightly the detection efficiency above some energy and to cause it to fall to nearly zero at about a gamma ray energy of 30 MeV for a point source. For a diffuse source such as the atmospheric background, the considerations are similar. Figure 4 shows the (area-time-detection efficiency) factor as a function of energy for a particular flight and potential source. The absolute value depends on the exposure time and the angle of the source with respect to the detector axis as a function of time, but the shape of the curve is only slightly sensitive to the direction of the source relative to the detector axis.

IV. RESULTS

(a) Galactic Center Region

In the introduction it was mentioned that, with an experiment on OSO-III, Clark, et al. (1968) detected gamma rays from the galactic plane with a flux which was strongest in the region near the galactic center. In an earlier paper, results of our group were published which set an upper limit for the flux from a point source assumed to be at the galactic center. The balloon flight data including the galactic center region have been reanalyzed in terms of a possible line source of finite width centered about the galactic plane. For reference Figure 5 shows a distribution of the arrival directions of the observed γ-rays with measured energies above 100 MeV. Most of these γ-rays are, of course,

atmospheric secondaries. Also shown in the figure are the contours of equal detecting efficiency and the galactic coordinates. From the figure it is seen that a region of the galactic plane from about -10° to +25° galactic longitude was examined. This is approximately the region of maximum intensity observed by Clark et al. (1969), wherein the average line intensity measured was (4.1 ±0.7) $\times 10^{-4}$ γ's/(cm^2 sec rad) in this region for energies greater than 100 MeV.

In the analysis of the balloon flight data obtained in the flight on Dec. 10, 1966, four different spatial intervals were examined; these were the region within the contour for 50% of maximum detection efficiency shown in Figure 5 from +15° to -15° galactic latitude, +10° to -10° galactic latitude, +5° to -5° galactic latitude, and +3° to -3° galactic latitude. For each region, the number of observed γ-rays above 100 MeV and above 150 MeV was determined. For the energy interval from 30 to 100 MeV, only the first three regions were studied, because the angular resolution of the γ-ray's arrival direction was not adequate to justify examining the smallest interval. From the flux calculated in this manner was subtracted the background gamma-ray flux, which was estimated from that observed in the region within the contour for 50% of maximum detection efficiency, but excluding the region within ±15° of the galactic center. The resulting flux was then converted to a line intensity and the results are shown in Table I, where the results of a simple subtraction with a one standard deviation error are given in Table Ia and two standard deviation upper limits are given in Table Ib. The results in Table I by themselves do not justify the claim of a detected flux, but the line intensity of (2.3 ±1.2) $\times$ 10^{-4} γ's/(cm^2 sec rad) above 100 MeV for the +3° to -3° interval is certainly consistent with a positive flux

11

Table Ia

Gamma Ray Line Intensity With One Standard Deviation Errors Along The Galactic Plane

From Galactic Longitude –10° to +25° In γ's/(cm^{2}sec rad)

Energy Interval	Galactic Latitude Interval			
	–15° to +15°	–10° to +10°	–5° to +5°	–3° to +3°
30 – 100 MeV	$0.9^{+2.2}_{-0.9} \times 10^{-4}$	$1.1^{+1.8}_{-1.1} \times 10^{-4}$	$0^{+1.0}_{-0} \times 10^{-4}$	—
> 100 MeV	$2.4^{+2.4}_{-2.4} \times 10^{-4}$	$(2.9 \pm 2.0) \times 10^{-4}$	$(2.2 \pm 1.4) \times 10^{-4}$	$(2.2 \pm 1.1) \times 10^{-4}$
> 150 MeV	$0^{+2.1}_{-0} \times 10^{-4}$	$0^{+1.7}_{-0} \times 10^{-4}$	$(1.2 \pm 1.2) \times 10^{-4}$	$(1.7 \pm 1.0) \times 10^{-4}$

Table Ib

Two Standard Deviation Upper Limits To Gamma Ray Line Intensity Along The Galactic Plane

From Galactic Longitude $-10°$ to $+25°$ In γ's/(cm²sec rad)

Energy Interval	Galactic Latitude Interval			
	$-15°$ to $+15°$	$-10°$ to $+10°$	$-5°$ to $+5°$	$-3°$ to $+3°$
30 – 100 MeV	$\leq 5.3 \times 10^{-4}$	$\leq 4.7 \times 10^{-4}$	$\leq 2.1 \times 10^{-4}$	—
>100 MeV	$\leq 7.2 \times 10^{-4}$	$\leq 6.7 \times 10^{-4}$	$\leq 5.0 \times 10^{-4}$	$\leq 4.4 \times 10^{-4}$
>150 MeV	$\leq 4.1 \times 10^{-4}$	$\leq 3.4 \times 10^{-4}$	$\leq 3.7 \times 10^{-4}$	$\leq 3.7 \times 10^{-4}$

and not in disagreement with a line intensity of $(4.1 \pm 0.7) \times 10^{-4}$ γ's/(cm^2 sec rad) observed in the OSO-III gamma ray experiment.

(b) Atmospheric Background

Figure 5 shows the flux of gamma rays above 100 MeV measured in this experiment as a function of zenith angle. Notice that the intensity rises from that at $\theta = 0$ (straight downward moving gamma rays) to a maximum near the horizon primarily because the average amount of material in which cosmic rays can produce gamma rays seen by the detector increases approximately as the secant of θ for small angles. A careful calculation must consider gamma ray absorption, source function variation with depth in the atmosphere, angular dependence, and other factors. The decrease in intensity after θ passes 90° is partly an energy effect. The gamma rays from $\pi°$ decay and other sources will be traveling at increasingly large angles with respect to the parent cosmic ray particles on the average and will therefore have an increasingly large relativistic decrease in their energy when their energy is transformed to the observor's reference frame. Hence, a larger and larger fraction of the gamma rays will have energies below 100 MeV. Also fewer gamma rays are formed along a line looking downward than along one looking at the horizon because a larger portion of the line is passing through a region with a lower gamma ray source function.

The changing shape of the energy spectrum as a function of θ is illustrated in Figure 7. In this figure, the γ-ray flux has been corrected for the detection efficiency as a function of energy, but not for the effect of detector energy resolution. The inclusion of the detector resolution affects the shape in only

minor respects. Notice that the spectra become steeper as θ increases, particularly at low energies.

The atmospheric gamma ray flux at 3 g/cm² was also integrated over the whole solid angle to compare it with the lower energy atmospheric photon spectra obtained with crystals which inherently integrate over all solid angles. The result is shown in Figure 8. It is seen that the gamma ray flux in the region from 30 to 200 MeV lies above the straight line extrapolation; this result is consistent with an enhancement expected in this energy interval as the result of decay of π°'s produced by collisions of cosmic rays with atmospheric nuclei.

An interesting comparison can be made between the balloon results discussed here and the OSO-III results for the upcoming gamma rays from the earth's atmosphere. The flux of γ-rays coming directly upwards is essentially the same at the balloon altitude of this experiment ($\sim$ 3 g/cm²) as it is outside the atmosphere, basically because the interaction mean free path of both the charged cosmic rays and gamma rays is large compared to 3 g/cm². At large angles with respect to the downward direction the flux measured at balloon altitude is no longer nearly the same as at a satellite altitude, and, of course, there is a downward moving flux of gamma rays at balloon altitudes produced by cosmic rays interacting in the atmosphere above the balloon.

The fluxes of upcoming gamma rays (E > 100 MeV) measured on Explorer 11 (Kraushaar et al., 1965) and on OSO-III (Clark, 1969) at corresponding geomagnetic latitudes are (1.9 ±0.5) × 10⁻³ and (10.5 ±1.0) × 10⁻³ gamma rays/(cm² sr sec) respectively. The flux measured in this work averaged over

15

approximately the same angles is $(3.7 \pm 0.8) \times 10^{-3}$ gamma rays/(cm^2 sr sec). Notice that the Explorer 11 results fall below the measurement reported here, but the OSO-III result is appreciably higher. The differences seem larger than would be expected on the basis of estimated errors, but are small compared to the difference of more than an order of magnitude between the galactic gamma ray flux observed by OSO-III and the predicted one.

The fluxes measured here may be compared to the downward fluxes measured in other balloon gamma ray experiments at similar altitudes. The results are displayed in Table II, and the agreement among these experiments is seen to be satisfactory, considering that the quoted errors of some of the experiments are only statistical.

(c) Search for a Discrete Source in Virgo

On February 27, 1968, the detector system was flown in an oriented gondola from Palestine, Texas, in a search for possible discrete sources in the direction of the Virgo cluster of galaxies. Particular emphasis was placed on examining the region about the radio galaxy M-87, recently observed to be an emitter of hard x-rays (Haymes, et al., 1968).

The celestial distribution of all gamma-rays observed during this exposure was determined under the assumption they were extraterrestrial in origin. The number of gamma-rays falling within a square angular bin with boundarier defined by the 95 percent confidence limits of angular uncertainty in gamma-ray arrival direction was determined for gamma-rays with energies greater than 100 MeV and 30-100 MeV.

16

Table II

Summary of the Downcoming Secondary Gamma Ray Flux Measurements at Balloon Altitudes*

Energy Interval	Atm. Depth (mb)	Meas. Flux $(cm^{-2}-sec^{-1}-sr^{-1})$	Linearly Extrapolated Flux to 3 mb $(cm^{-2}-sec^{-1}-sr^{-1})$	Reference
> 30 MeV	3.5	$(5.2 \pm 0.5) \times 10^{-3}$	$(4.5 \pm 0.4) \times 10^{-3}$	Frye & Smith (1966)
> 30 MeV	2.3	$(3.7 \pm 0.4) \times 10^{-3}$	$(4.8 \pm 0.5) \times 10^{-3}$	Frye & Wang (1968)
> 30 MeV	3.0	$(5.7 \pm 0.6) \times 10^{-3}$	$(5.7 \pm 0.6) \times 10^{-3}$	Present Results
$\gtrsim$ 50 MeV	8.5	$(2.0 \pm 0.2) \times 10^{-2}$	$(7.0 \pm 0.7) \times 10^{-3}$	Cline (1961)
> 50 MeV	3.0	$(4.8 \pm 0.5) \times 10^{-3}$	$(4.8 \pm 0.5) \times 10^{-3}$	Present Results
> 100 MeV	6.5	$(4.3 \pm 0.2) \times 10^{-3}$	$(2.0 \pm 0.1) \times 10^{-3}$	Cobb et al. (1965)
> 100 MeV	4.0	$(1.9 \pm 0.2) \times 10^{-3}$	$(1.4 \pm 0.2) \times 10^{-3}$	Fazio et al. (1968)
> 100 MeV	3.0	$(3.0 \pm 0.4) \times 10^{-3}$	$(3.0 \pm 0.4) \times 10^{-3}$	Present Results

*The detectors in all cases sampled a region of the sky within about 30° from the vertical.

The observed intensity of atmospheric secondary gamma rays was 5.7×10^{-3} gamma rays/cm^2 sec ster for $30 \leq E_\gamma \leq 100$ MeV and 6.5×10^{-3} gamma rays/cm^2 sec ster for $E_\gamma > 100$ MeV. The rather high intensity observed for measurements at an atmospheric depth of 3 g/cm^2 results from the fact that a malfunction in the orientation system caused the detector axis to tilt to an angle of 45° with respect to the vertical.

For the intensities quoted above, the expected number of gamma-rays in the squares of uncertainty are N_B (30-100) $= 2.0$ and N_B (> 100) $= 0.6$. The observed number are N_0 (30-100) $= 3.0$ and N_0 (> 100) $= 2.0$. The 95% confidence limits on the number of source counts, S, are then given by the relationship (see Appendix II).

$$\sum_{N=0}^{N_0} \frac{(N_B + S)^N e^{-(N_B+S)}}{N!} \Bigg/ \sum_{N=0}^{N_0} \frac{N_B^N e^{-N_B}}{N!} = .05 \qquad (5)$$

The 95 percent confidence limits obtained are 3.2×10^{-4} gamma rays/cm^2 sec for $30 \leq E_\gamma \leq 100$ MeV and 2.2×10^{-4} gamma rays/cm^2 sec for $E_\gamma > 100$ MeV. These limits, more than an order of magnitude higher than the capability of the detector system, resulted from the failure in the orientation system. This failure resulted in poor orientation and eventually a total loss of data after only 1.5 hours of exposure.

(d) Summary of Upper Limits on Discrete Sources

The limits obtained from all flights have been reanalyzed in two energy bins and are presented in Table III. For comparison, the best existing limits of previously reported data are included.

Clark et al. (1968) suggest that possibly a substantial part of the observed galactic gamma ray intensity is due to unresolved discrete sources. Ögelman (1969) has subsequently shown that there is reasonably good agreement between the observed dependence on galactic longitude of the line intensity of gamma-rays > 100 MeV observed by Clark et al. (1968) and the distribution of x-ray sources in the galactic plane. Table III includes a column containing the gamma-ray fluxes expected from the indicated sources if the observed hard x-ray spectra were extrapolated to gamma-ray energies. For those sources for which the spectra is not well determined, the x-ray fluxes in the 1 to 10 Å region listed in the Friedman (1967) survey have been extrapolated using the $E^{-2.0}$ relationship suggested by Ögelman (1969). No extrapolation is made for the apparently thermal source Sco XR-1 nor for sources not known to be x-ray emitters.

ACKNOWLEGEMENT

Table III

Discrete Source Limits

Source	95% Confidence Limit (This Work) (cm⁻² sec⁻¹)		Limit (Other Work) (cm⁻² sec⁻¹)		X-Ray Extrapolation (cm⁻² sec⁻¹)	
	$30 - 100$ MeV	>100 MeV	> 50 MeV	> 100 MeV	$30 - 100$ MeV	> 100 MeV
Crab Nebula	2.7×10^{-4}	1.8×10^{-4}		3.1×10^{-5} (1)	2.1×10^{-4} (4)	1.1×10^{-4} (4)
Centaurus A	6.3×10^{-5}	6.4×10^{-5}	3.0×10^{-4} (3)			
Quiet Sun	1.3×10^{-4}	3.8×10^{-5}		7.4×10^{-5} (1)		
Sco XR-1	8.8×10^{-5}	3.8×10^{-5}				
Sco X-1	8.8×10^{-5}	3.8×10^{-5}				
Galactic Center	7.1×10^{-5}	5.1×10^{-5}	5.3×10^{-4} (3)			
Oph XR-1	6.1×10^{-5}	5.1×10^{-5}			5.1×10^{-5} (6)	2.2×10^{-5} (6)
Oph XR-2	1.2×10^{-4}	6.5×10^{-5}			1.9×10^{-5} (6)	8.3×10^{-6} (6)
Sgr XR-1	8.8×10^{-5}	5.1×10^{-5}			6.2×10^{-5} (6)	2.7×10^{-5} (6)
Sgr XR-2	1.0×10^{-4}	6.5×10^{-5}			6.2×10^{-5} (6)	2.7×10^{-5} (6)
Moon	1.2×10^{-4}	5.1×10^{-5}				
Virgo (M-87)	3.2×10^{-4}	2.2×10^{-4}	1.0×10^{-5} (2)		6.7×10^{-5} (5)	5.3×10^{-5} (5)

(1) Fazio, et al. (1968).

(2) Frye and Wang (1968).

(3) Kraushaar et al. (1965).

(4) Extrapolated from X-ray energies using the spectrum of Peterson, et al. (1968).

(5) Extrapolated from X-ray energies using the spectrum of Haymes, et al. (1968).

(6) Extrapolated from 1-10 Å X-ray fluxes (Friedman, 1966) as described in text.

APPENDIX I

CALCULATION OF WEIGHTING FACTOR
FOR GAMMA-RAY ARRIVAL DIRECTION

Pinkau (1968) has shown that, for a set of k spark readings, x_{ni} recorded

at levels z_n in the spark chamber, the relative probability of x' and ϕ', the

initial coordinate and angle with respect to the spark chamber axis, is given by

$$P(y',\phi') = \prod_{i=1}^{k} \frac{1}{\sqrt{\pi(\xi_d^2 W_{ni} + 2\alpha^2)}} \exp \left[-\frac{(x_{ni} - x' - i\Delta\phi')^2}{(\xi_d^2 W_{ni} + 2\alpha^2)} \right] \quad \text{(A-1)}$$

where ξ_d^2 and W_{ni} are complicated expressions involving the composition of the

scattering plates and the geometry of the detector and α, the root mean square

reading error in the spark position. For our detector

$$\xi_d^2 W_{ni} \approx \frac{2.89}{(E_e)^2} \left(\frac{n^3}{3} - \frac{n}{12} \right) \quad \text{(A-2)}$$

where n is the number of plates through which the electron has passed between

readings. For $\xi_d^2 W_{ni} << 2\alpha^2$, it is clear that $P(x', \phi')$ is maximum for a minimum

value for the numerator of the argument of the exponent $\sum_{i=1}^{k} (x_{ni} - x' - i\Delta\phi')^2$.

This is by definition the least squares fit to the spark chamber data points,

giving x'_{max} and ϕ'_{max}.

Pinkau has further shown that, integrating over x', the distribution function

may now be expressed as

$$P(\phi', \phi'_{max}) \; \alpha \; e^{-\frac{\delta^2}{\sigma^2}} \tag{A-3}$$

where

$$\delta = \Delta(\phi' - \phi'_{max}) \tag{A-4}$$

and

$$\sigma = \sqrt{\frac{12}{k^3 - k} \; (\xi_d^2 \, W_{ni} + 2a^2)} \tag{A-5}$$

where we have neglected energy loss in the plates.

The distribution for the two electrons of a pair is then given by

$$(p_1) \, (p_2) \; \alpha \; \exp \left[-\frac{\delta_1^2}{\sigma_1^2} - \frac{\delta_2^2}{\sigma_2^2} \right] \tag{A-6}$$

where

$$\delta_{1,2} = \Delta(\phi' - \phi'_{1,2 \, max}) $$

and this distribution is maximized with respect to ϕ'_{max} for

$$\frac{\partial \ln(p_1 p_2)}{\partial \phi'} = 0 \, . \tag{A-7}$$

Hence

$$\frac{\delta_1}{\sigma_1^2} = -\frac{\delta_2}{\sigma_2^2} \, , \tag{A-8}$$

yielding

$$\phi'_{max} = \frac{\phi'_{2max} \, \sigma_1^2 + \phi'_{1max} \, \sigma_2^2}{\sigma_1^2 + \sigma_2^2} \, .$$

(A-9)

APPENDIX II

CALCULATION OF UPPER LIMITS

In any balloon exposure in search of a discrete source of gamma rays, a celestial distribution is obtained from the determination of the arrival direction of each observed gamma-ray. Most of the observed quanta result from secondary gamma rays produced by the interaction of energetic charged particle cosmic rays with the matter in the atmosphere above the detector. In an angular bin surrounding the source, determined by the accuracy with which the gamma ray arrival direction can be determined, N_B counts will be observed. From the overall distribution of arrival directions, assumed to be dominated by secondaries, and average value N_B of atmospheric produced gamma rays would be expected in the bin. The probability that a given N_B and assumed average source strength s will give the number of observed counts N_0 is given by

$$P(s) = \sum_{i=0}^{N_0} \frac{e^{-s} s^i}{i!} \frac{e^{-N_B} N_B^{N_0-i}}{(N_0 - i)!} = \frac{e^{-(N_B+s)} (N_B + s)^{N_0}}{N_0!} . \qquad (A-10)$$

The 95% probability that an average source strength s_u or less with a distribution P(s) will give the observed number of counts is given by:

$$\frac{\int_{s_u}^{\infty} P(s) \, ds}{\int_{0}^{\infty} P(s) \, ds} = \frac{\sum_{i=0}^{N_0} \frac{e^{-(s_u + N_B)} (s_u + N_B)^i}{i!}}{\sum_{j=0}^{N_0} \frac{e^{-N_B} N_B^j}{j!}} = .05 \qquad (A-11)$$

This equation is the same as that used by Hearn (1968).

24

We feel that this equation gives the best possible estimate of the upper limit on the average source strength with the available data since there is insufficient information to determine whether fluctuations from the expected values are due to variations in the source contribution or the background contribution.

REFERENCES

Bethe, H., 1953, Phys. Rev. $\underline{89}$, 1256.

Clark, G. W., G. P. Garmire, and W. L. Kraushaar, 1968, Ap. J. $\underline{153}$, L203.

Clark, G. W., G. P. Garmire, and W. L. Kraushaar, 1969, private communication.

Cline, T., 1961, Phys. Rev. Letters $\underline{7}$, 109.

Cobb, R., J. G. Duthie, and J. Stewart, 1965, Phys. Rev. Letters $\underline{15}$, 507.

Ehrmann, C. H., C. E. Fichtel, D. A. Kniffen, and R. W. Ross, 1967, Nuclear
    Instruments and Methods $\underline{56}$, 109.

Fazio, G. G., H. F. Helmken, S. J. Cavrak, and D. R. Hearn, 1968, Can. J. Phys.,
    $\underline{46}$, S427.

Fichtel, C. E., T. L. Cline, C. H. Ehrmann, D. A. Kniffen, and R. W. Ross, 1968,
    Canadian Journal of Physics $\underline{46}$, S419.

Fowler, P. H., 1966, Phil. Mag. $\underline{XLI}$, 169.

Friedman, H., E. T. Byram, and T. A. Chubb, 1967, Science, $\underline{156}$, 374.

Frye, Jr., G. M., and L. H. Smith, 1966, Phys. Rev. Letters $\underline{17}$, 733.

Frye, Jr., G. M., and C. P. Wang, 1968, Can. J. Phys., $\underline{46}$, S448.

Goudsmit, S., and J. L. Saunderson, 1940, Phys. Rev. $\underline{57}$, 24.

Haymes, R. C., D. V. Ellis, G. J. Fishman, S. W. Glenn, and J. D. Kurfess, 1968, Ap. J. Letters, 151, L125.

Hearn, D. R., 1968, Smithsonian Astrophysical Observatory Spec. Rep. No. 277.

Kniffen, D. A., 1967, Ph.D. Thesis, Catholic University.

Kraushaar, W. L., G. W. Clark, G. Garmire, H. Helmken, P. Higbie, and M. Agogino, 1965, Ap. J. 141, 845.

Molière, G., 1947, Zeitschrift fur Naturforschung IIa, 133.

Molière, G., 1948, Ibid, IIIa, 78.

Molière, G., 1955, Ibid, Xa, 177.

Ögelman, H., 1969, Nature, in press.

Peterson, L. E., A. S. Jacobson, R. M. Pelling, and D. A. Swartz, Can. J. Phys., 46, S437.

Pinkau, K., 1966, Zeitschrift fur Physik XCCVI, 163.

Pinkau, K., 1967, Nuclear Instruments and Methods 57, 173.

Pinkau, K., 1968, Investigation of Spark Chamber Systems with Respect to Power of Resolution in Energy, Position, and Direction, Max-Planck-Institut für Physik und Astrophysik Preprint.

Scott, W. T., 1952, Phys. Rev. 84, 245.

Snyder, H., and W. T. Scott, 1949, Phys. Rev. 76, 220.

Stearns, M., 1949, Phys. Rev. 76, 836.

Williams, E. J., 1939, Proceedings of the Royal Society of London CLXIX, 531.

FIGURE CAPTIONS

Figure 1. Schematic drawing of digitized spark chamber gamma-ray telescope.

Figure 2. Scattering coordinates and parameters in the spark chamber.

Figure 3. Uncertainty in gamma ray arrival direction — 95% confidence as a function of energy.
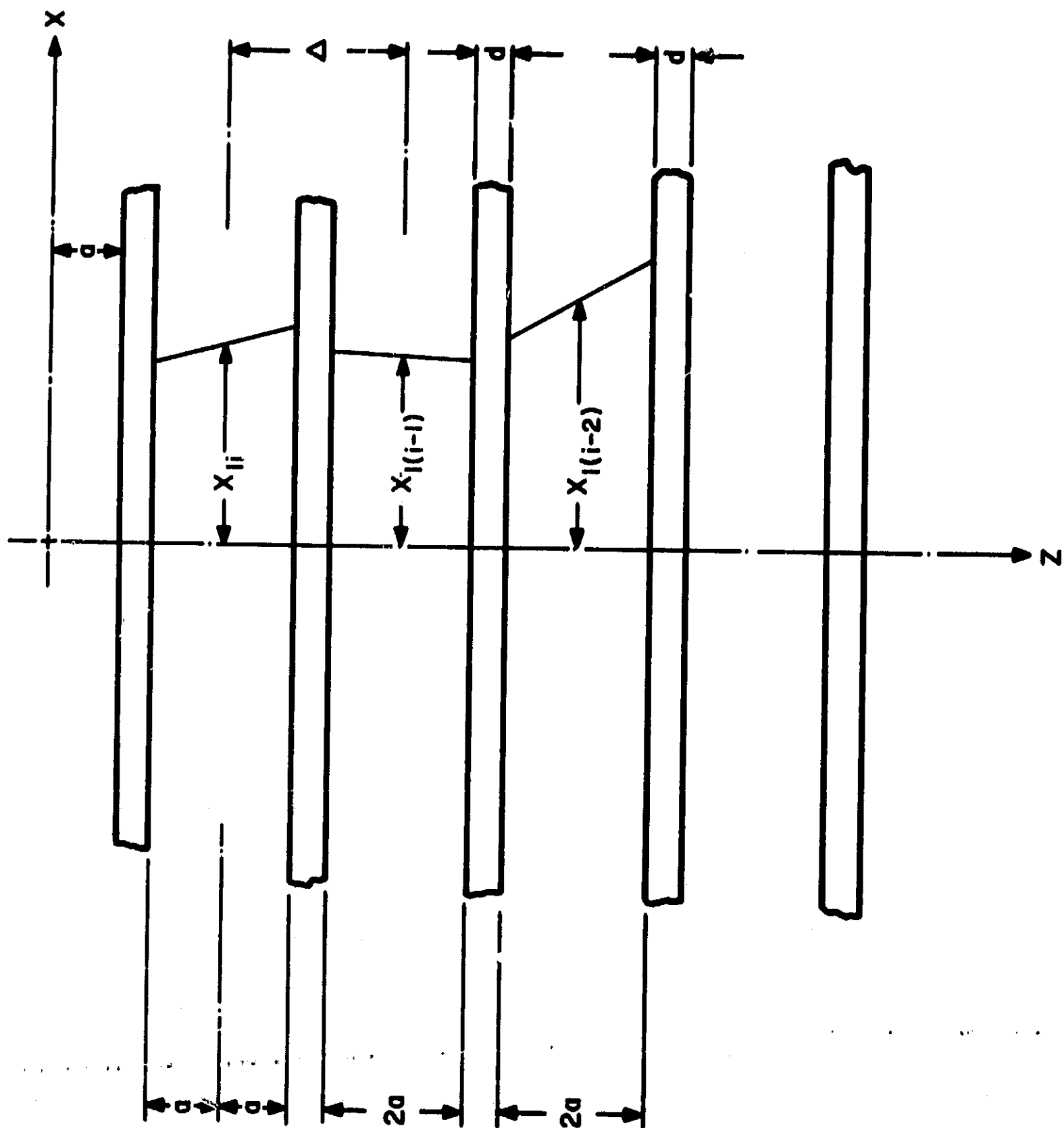
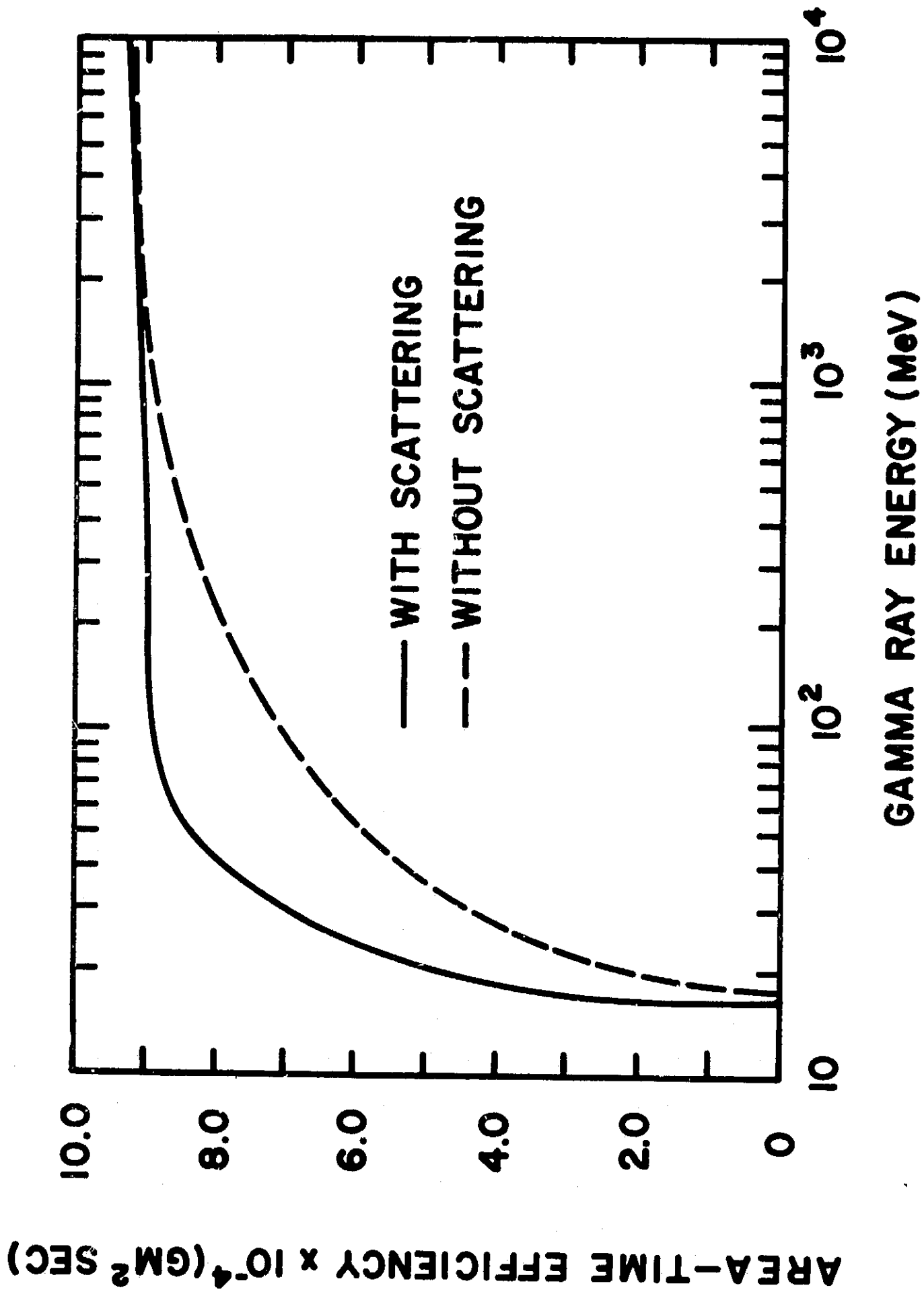Figure 4. Area-time-detection efficiency factor as a function of energy.

Figure 5. Distribution of the arrival directions of the observed gamma-rays with measured energies above 100 MeV. The dark lines represent the indicated galactic latitude, and the galactic longitude is indicated by marks along the 0° galactic latitude line. The dashed curves are contours of equal area-solid angel-collection time and the numbers by these curves indicate the percentage of the maximum area-solid angle-collection time for this flight.

Figure 6. Gamma-ray flux at a balloon altitude of 3 g/cm^2 as a function of the angle with respect to the vertical.

Figure 7. Energy spectrum of gamma rays observed at a balloon altitude of 3 g/cm^2 as a function of the angle with respect to the vertical.

Figure 8. Energy spectrum of atmospheric background gamma-ray flux integrated over all solid angles.

GAMMA RAY ENERGY (MeV)

AREA-TIME EFFICIENCY x 10⁻⁴ (GM² SEC)

— WITH SCATTERING
--- WITHOUT SCATTERING

UNCERTAINTY IN ARRIVAL DIRECTION.
95 % CONFIDENCE LEVEL (DEGREES)

GAMMA RAY ENERGY (MeV)

ATMOSPHERIC GAMMA RAY
SPECTRUM
3.5 G/CM² λ = 40°

PETERSON & SCHWARTZ

THIS EXPERIMENT

(OPENING ANGLE)

GUARD SCINTILLATION
COUNTER

CUT AWAY OF
UPPER SPARK
CHAMBER
(WIRES NOT TO
SCALE)

SCINTILLATOR AND
LIGHT PIPE HOUSING

LIGHT PIPE

LOWER SPARK
CHAMBER

PHOTO-MULTIPLIER
TUBE HOUSING

PHOTO-MULTIPLIER
TUBE

PHOTO-MULTIPLIER
TUBE

CERENKOV COUNTER
HOUSING